Density functional approach for the magnetism of #-TeVO[subscript 4]

Density functional approach for the magnetism of β-$TeVO_4$

A. Saúl*

Aix-Marseille University, CINaM-CNRS UMR 7325 Campus de Luminy, 13288 Marseille cedex 9, France and Department of Civil and Environmental Engineering, Massachusetts Institute of Technology, and MultiScale Material Science for Energy and Environment, UMI 3466 CNRS-MIT, 77 Massachusetts Avenue, Cambridge, Massachusetts 02139, USA

G. Radtke

Institut de Minéralogie, de Physique des Matériaux, et de Cosmochimie (IMPMC) Sorbonne Universités–UPMC Université de Paris 06, UMR CNRS 7590, Muséum National d'Histoire Naturelle, IRD UMR 206, 4 Place Jussieu, F-75005 Paris, France

(Received 22 December 2013; revised manuscript received 3 February 2014; published 17 March 2014)

Density functional calculations have been carried out to investigate the microscopic origin of the magnetic properties of β-$TeVO_4$. Two different approaches, based either on a perturbative treatment of the multiorbital Hubbard model in the strongly correlated limit or on the calculation of supercell total energy differences, have been employed to evaluate magnetic couplings in this compound. The picture provided by these two approaches is that of weakly coupled frustrated chains with ferromagnetic nearest-neighbor and antiferromagnetic second-nearest-neighbor couplings. These results, differing substantially from previous reports, should motivate further experimental investigations of the magnetic properties of this compound.

DOI: 10.1103/PhysRevB.89.104414 PACS number(s): 75.30.Et, 75.10.Dg, 71.20.Lp

I. INTRODUCTION

Oxides involving tetravalent vanadium in square-pyramidal or octahedral coordination provide numerous examples of open structures where the transition-metal coordination polyhedra share either corners or edges to form low-dimensional frameworks [1]. Low dimensionality as well as pronounced quantum fluctuations expected for spin-$\frac{1}{2}$ systems are often at the origin of unconventional magnetic properties in vanadates [2–6]. These properties are largely governed by the signs and amplitudes of exchange interactions occurring between localized magnetic moments. A straightforward application of Goodenough-Kanamori-Anderson rules [7–10] is often greatly hindered by the complex geometry met in these compounds. This is first due to strong distortions of the V^{4+} coordination octahedra, often better described as square pyramids and characterized by a large dispersion of the V-O bond lengths. It is also related to the weak π interaction between O-p and V-d_{xy} orbitals [11] mediating kinetic superexchange mechanisms. As a result, a situation is often met where ferromagnetic (FM) and antiferromagnetic (AFM) contributions are balanced and the sign of the resulting exchange interaction is impossible to predict solely on the basis of simple geometrical considerations.

The structure of β-$TeVO_4$ was first reported in 1973 by Meunier *et al.* [12] as a high-temperature polymorph of $TeVO_4$, and despite its potentially interesting geometry as a low-dimensional spin-$\frac{1}{2}$ system, it has not received much attention in almost 40 years. This vanadate crystallizes in the monoclinic structure shown in Fig. 1(a) where V^{4+} are located inside corner-sharing square pyramids forming zigzag chains running along the crystal c axis. These chains are well separated from each other by the large Te^{4+} ions and are stacked along the crystal a axis. Apical oxygens of the square pyramids are all pointing in the same direction within a given chain. However, the two adjacent chains contained in the crystal unit cell are alternatively pointing above and below the (b,c) plane. The specific geometry of the zigzag chains in β-$TeVO_4$ is fairly rare in vanadates and could be at the origin of interesting magnetic properties. In addition to nearest-neighbor interaction [J_1 in Fig. 1(b)], the arrangement of the V^{4+} coordination pyramids is indeed favorable to the occurrence of second-nearest-neighbor interactions along the chain [J_4 in Fig. 1(b)] through V-O-O-V exchange paths [13] and could therefore promote β-$TeVO_4$ as a potential realization of the J-J' (first and second nearest neighbor) chain model. The determination of the signs and strengths of these couplings, as well as other potential interchain interactions, is however far from obvious.

From an experimental point of view, the first in-depth reports of the magnetic properties of β-$TeVO_4$ have been published only very recently [13,14] and emphasize the complex behavior of this compound. The temperature dependence of the magnetic susceptibility, showing a broad maximum at about 14 K, has been investigated carefully by Savina *et al.* [13] and eventually interpreted as that of a uniform antiferromagnetic spin-$\frac{1}{2}$ chain with a single exchange coupling. Attempts to extend this analysis beyond a one-dimensional model only showed that the strength of additional couplings does not exceeds a few kelvins [13]. However, these results contrast with the slightly positive Curie-Weiss temperature obtained by fitting the high-temperature range (150–400 K) of the magnetic susceptibility, which tends to support the presence of weak ferromagnetic or at least balanced interactions in this compound. The occurrence of a broad crossover ($T_{cros} \approx$ 130 K) separating two magnetic regimes dominated either by ferromagnetic correlations at high temperature or by antiferromagnetic correlations at low temperature has been proposed [13]. This crossover has recently been interpreted as a consequence of a V^{4+} orbital reordering associated with a shift of the transition-metal ion away from the apical oxygen inside its coordination square pyramid [14]. Finally, a series of low-temperature magnetic phase transitions has been observed and attributed to the occurrence of a first long-range-ordered

*saul@cinam.univ-mrs.fr

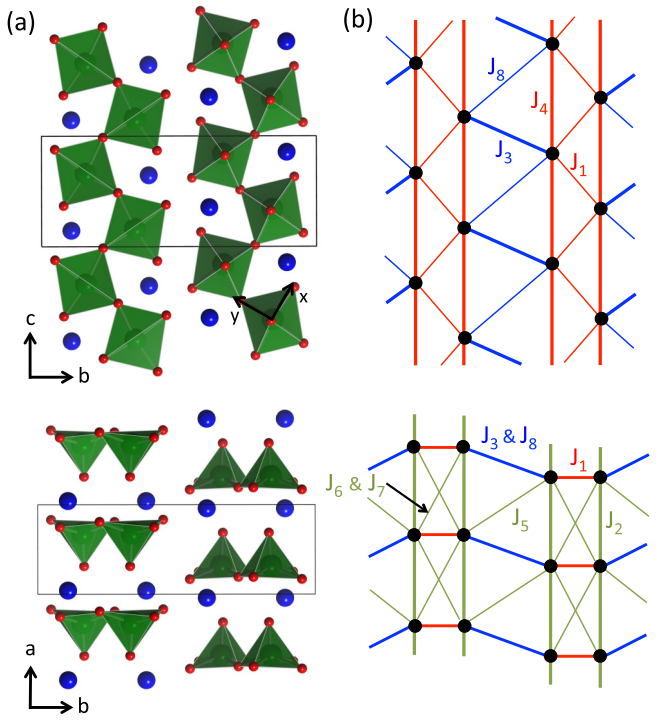

FIG. 1. (Color online) (a) Crystal structure of β-$TeVO_4$. The coordination square pyramids of vanadium are shown in green, oxygen ions are in red, and tellurium ions are in blue. The crystal unit cell is also represented. (b) Magnetic couplings in β-$TeVO_4$ up to the eighth nearest neighbor. Couplings occurring within the chains are represented in red (J_1 and J_4), couplings between chains in the (b,c) planes are represented in blue (J_3 and J_8), and couplings between chains of distinct (b,c) planes are represented in green (J_2, J_5, J_6, and J_7).

antiferromagnetic state ($T_N \approx 4.65$ K) followed by subsequent spin rearrangements [13].

In this paper, the electronic structure and the magnetic properties of β-$TeVO_4$ are investigated on the basis of density functional calculations. The picture emerging from this work differs substantially from the uniform AFM spin-$\frac{1}{2}$ chain model proposed earlier [13]. These calculations indeed support the model of weakly coupled frustrated chains where dominant intrachain interactions are (i) *ferromagnetic* for the nearest-neighbor couplings [J_1 in Fig. 1(b)] and (ii) *antiferromagnetic* for second-nearest-neighbor couplings [J_4 in Fig. 1(b)]. The above-mentioned hypothesis based on a temperature-induced orbital reordering is also discussed.

II. COMPUTATIONAL DETAILS

Band structure calculations and total energy calculations were performed with the QUANTUM ESPRESSO [15] and WIEN2K [16] codes. These codes are based on density functional theory and use respectively the pseudopotential plane-wave and the full-potential linearized augmented plane-wave plus local orbitals (FP-LAPW+lo) methods.

QUANTUM ESPRESSO calculations were performed using ultrasoft pseudopotentials [18] with plane-wave and charge-density cutoff of 40 Ry and 400 Ry, respectively. Maximally localized Wannier function (MLWF) interpolation of the band structure was calculated using WANNIER90 [19] interfaced with QUANTUM ESPRESSO. With this code, the generalized gradient approximation of Perdew, Burke, and Ernzerhof (GGA-PBE) [17] has been employed for exchange and correlation.

WIEN2K calculations were performed with a cutoff parameter $RK_{max} = 7$ and muffin-tin sphere radii set to 1.74 a.u. for Te, 1.61 a.u. for V, and 1.42 a.u. for O. Besides the generalized gradient approximation of Perdew, Burke, and Ernzerhof (GGA-PBE) [17] two different DFT+U implementations [20] based either on the "around-mean-field" (AMF) [21] or on the "self-interaction-correction" (SIC) [22] schemes were employed. A value of $U_{eff} = 4$ eV, reasonable for V^{4+} ions [6,23,24], was used in both approaches. Hybrid PBE0 [25] was also used. As in the case of DFT+U calculations, its use was however restricted to the subspace spanned by states corresponding to strongly correlated electrons [26,27], i.e., the V-3d states.

Total energy calculations were performed with WIEN2K because of the high accuracy of the FP-LAPW+lo and the availability of different implementations of DFT+U. They have been carried out using the experimental crystal structure determined by Meunier *et al.* [12]. In order to assess the effect of the structure on the magnetic couplings, structural relaxation was carried out with QUANTUM ESPRESSO and supercell total energies recalculated with WIEN2K. The consistency of the results obtained with these two codes was verified systematically for calculations performed with the GGA-PBE exchange-correlation functional.

III. RESULTS AND DISCUSSION

A. Model Hamiltonian approach

The density of states and band structure of paramagnetic β-$TeVO_4$ are shown in Figs. 2(a) and 2(b), respectively. The valence band of this compound extends over a 7 eV range from about -10 to -3 eV and is largely dominated by the O-2p states. The four half-filled V^{4+} states of d_{xy} symmetry (the monoclinic $P2_1/c$ unit cell contains four formula units), responsible for the magnetic properties of this compound, are very well separated from this valence band located at lower energy, as well as from the remaining crystal-field-split V-3d states at higher energy. This result illustrates clearly the strong crystal-field stabilization of the V-d_{xy} states in a square pyramid environment. Indeed, a second group of eight bands is found with a dominant V-d_{xz} and V-d_{yz} character at about 1 eV above the Fermi level, i.e., above the V-d_{xy} states. Although a nonnegligible hybridization with the Te-5p states occurs in this energy range, these bands are largely dominated by their V-3d component. The weight of the Te-5p states increases starting from 1.5 eV above the Fermi level, i.e., in the high-energy region where antibonding states of V-$d_{x^2-y^2}$ and V-d_{z^2} character are also found. In a first approach, we evaluated the magnetic couplings through a mapping of this paramagnetic band structure onto a modified Kugel-Khomskii model [23,28,29]. This mapping has been performed first by computing a set of twelve MLWFs following the method of Marzari and Vanderbilt [30] and spanning the twelve bands of

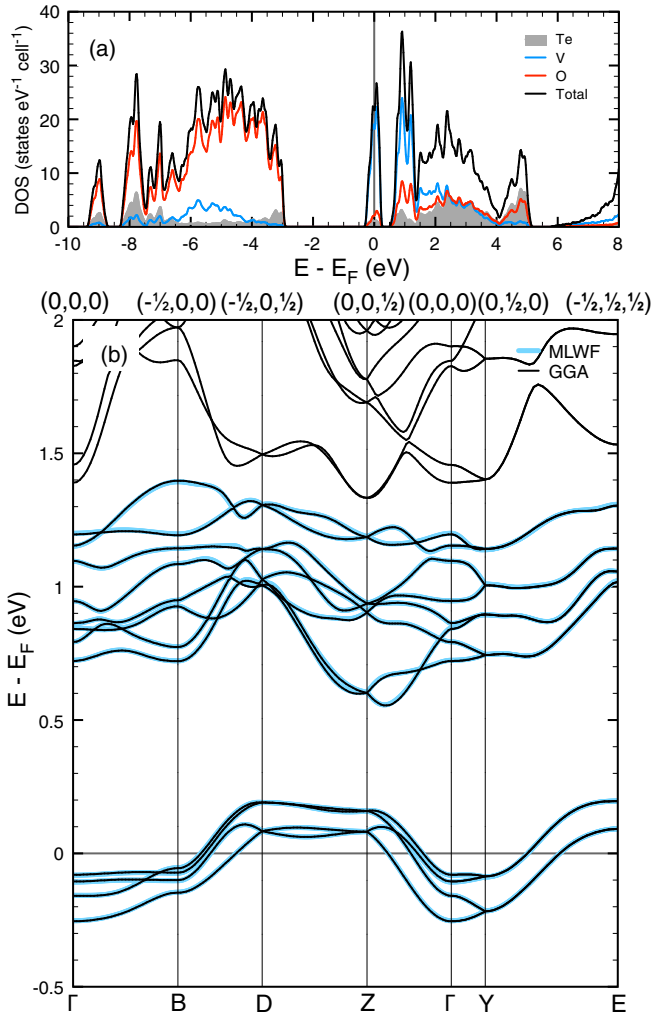

FIG. 2. (Color online) Nonmagnetic GGA-PBE electronic structure of β-$TeVO_4$. (a) Total and projected densities of states and (b) DFT-GGA (black solid line) and Wannier-interpolated (in blue) band structure of β-$TeVO_4$. The high-symmetry point coordinates in the Brillouin zone are given in units of the reciprocal lattice basis vectors of the monoclinic $P2_1/c$ unit cell.

dominant V-d_{xy}, d_{xz}, and d_{yz} character located between -0.3 and 1.5 eV. The Wannier-interpolated band structure obtained following this procedure is superimposed on the DFT-GGA band structure in Fig. 2(b). It should be noted here that these MLWFs are not eigenstates of the on-site (crystal-field) part of the Hamiltonian, as assumed in the Kugel-Khomskii model, even though they are already very close in this particular case. In order to correct this point, a diagonalization was performed and the hopping integrals provided in the output of WANNIER90 were recalculated accordingly. Hopping integrals obtained through this first step were then employed in the following expression of the magnetic couplings [29]:

$$J_i = \frac{4\left(t^{(i)}_{xy,xy}\right)^2}{U} - \sum_{m=xz,yz} \frac{4\left(t^{(i)}_{xy,m}\right)^2 J_H}{(U+\Delta_m)(U+\Delta_m-J_H)}. \quad (1)$$

In this expression, U is the on-site Coulomb term, J_H is the intra-atomic exchange interaction, Δ_m is the energy difference between half-filled (d_{xy}) and empty (d_{xz},d_{yz}), low-lying (at about 1 eV above the Fermi level) vanadium orbitals and $t^{(i)}_{xy,m}$ are the corresponding hopping integrals. The first term of this expression arises from the interaction between half-filled, magnetically active, V-d_{xy} orbitals and is antiferromagnetic in nature. On the contrary, the second term favors a ferromagnetic alignment of the moments through the interaction between half-filled and empty, low-lying d_{xz} and d_{yz} orbitals. In the following, we will restrict our analysis to this three-band model mainly because V-d_{z^2} and $d_{x^2-y^2}$ bands arise at much higher energies (between 1.5 and 4 eV above the Fermi level) and strongly hybridize with the Te-5p states. Numerical results obtained using on-site energies and hopping integrals between MLWFs in Eq. (1) together with $U = 4$ eV and $J = 1$ eV typically employed for V^{4+} ions [23,29,31] are given in Table I. A clear and somewhat surprising picture arises from these results: as expected, dominant magnetic couplings in β-$TeVO_4$ happen along the zigzag chain but the largest interaction corresponds to the second-nearest-neighbor interaction (J_4) and is antiferromagnetic whereas the nearest-neighbor interaction (J_1) is weaker and ferromagnetic. Interchain couplings are antiferromagnetic and much weaker in amplitude as could be anticipated from the weak dispersion of the V-d_{xy} bands along $\Gamma \rightarrow B$, $D \rightarrow Z$, or $\Gamma \rightarrow Y$. The image of the magnetism of β-$TeVO_4$ given by this approach is therefore that of weakly coupled frustrated ferromagnetic chains. The most striking result, namely that J_1 is predicted to be ferromagnetic, arises from a weak hopping integral between neighboring V-d_{xy} orbitals along the chain. If one neglects any other interaction than the first- and second-nearest-neighbor interactions along the chains, the energy dispersion of the V-d_{xy} bands in β-$TeVO_4$ are given by

$$\epsilon(\vec{k}) = \epsilon_{xy} \pm 2t^{(1)}_{xy,xy}\cos\pi k_3 + 2t^{(4)}_{xy,xy}\cos 2\pi k_3, \quad (2)$$

where $\vec{k} = (k_1,k_2,k_3)$ is the adimensional reciprocal vector in units of the reciprocal lattice basis vectors. Qualitatively, the V-d_{xy} bands, shown in Fig. 2(b), present a dependence along $B \rightarrow D$, $Z \rightarrow \Gamma$, or $Y \rightarrow E$. They are clearly dominated by the last term of Eq. (2) ($\propto \cos 2\pi k_3$) indicating that $|t^{(4)}_{xy,xy}| > |t^{(1)}_{xy,xy}|$. In order to understand this result, it is instructive to look at the shape of the MLWF of dominant V-d_{xy} character shown in Fig. 3. It can be seen that the tails of the Wannier function on the 2p states of the two bridging oxygens forming

TABLE I. Magnetic couplings up to the eighth nearest neighbor calculated using Eq. (1) with $U = 4$ eV, $J = 1$ eV, on-site energies, and hopping integrals from MLWF calculations. According to the convention used in Eq. (1), positive couplings correspond to AFM interactions.

	distance (Å)	J^{AFM}	J^{FM}	J
J_1	3.642	5	−23	−18
J_2	4.379	0	0	0
J_3	4.915	6	−2	4
J_4	5.446	49	−1	48
J_5	5.476	13	−1	12
J_6	5.633	0	−1	−1
J_7	5.758	1	0	1
J_8	5.935	0	0	0

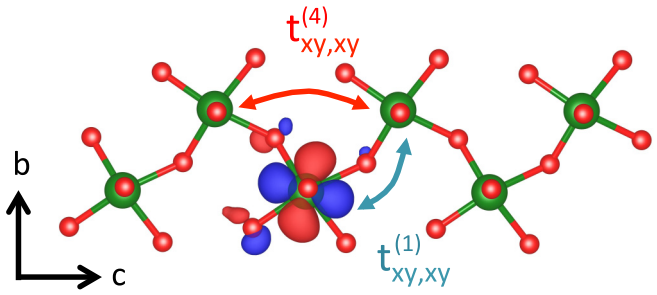

FIG. 3. (Color online) MLWF of dominant V-d_{xy} character calculated with WANNIER90 in β-$TeVO_4$. Antibonding $2p$ tails on neighboring oxygens are also clearly visible.

the chain are not symmetric but with a larger weight on the nearest oxygen (the V-O distance is 1.927 Å compared to 2.034 Å for the second bridging oxygen). The alternating V-O bond lengths along the chain are therefore responsible for the small overlap between Wannier functions centered on adjacent sites and, thus, for the small hopping integral $t^{(1)}_{xy,xy}$ ($\sim$20 meV) leading to a weak AFM component for J_1. The FM component therefore dominates through nonnegligible hopping between half-filled and empty orbitals ($t^{(1)}_{xy,xz} \sim 84$ meV and $t^{(1)}_{xy,yz} \sim -46$ meV). These results, although qualitative, differ from the image originally drawn from the analysis of the experimental magnetic susceptibility [13] and as such, require further investigations. A second method, based on the calculation of supercell total energy differences and allowing for an independent evaluation of the magnetic couplings, has thus been employed.

B. Supercell total energy approach

The calculation of magnetic couplings can be carried out within the broken symmetry formalism, i.e., by mapping total energies corresponding to various collinear spin arrangements within a supercell onto a Heisenberg Hamiltonian

$$\hat{H} = \hat{H}_0 + \sum_{i>j} J_{ij}\, \hat{\mathbf{S}}_\mathbf{i} \cdot \hat{\mathbf{S}}_\mathbf{j}, \tag{3}$$

where $\hat{H}_0$ is the spin-independent part of the Hamiltonian, J_{ij} are the magnetic couplings to determine, and $\hat{\mathbf{S}}_\mathbf{i}$ and $\hat{\mathbf{S}}_\mathbf{j}$ are, in our case, the $S = 1/2$ spin operators localized on V^{4+} ions located at site i and j respectively. It is straightforward to show that the expectation value of Hamiltonian (3) on a DFT state $|\alpha\rangle$ (obtained by preparing the initial electron density according to a particular collinear spin arrangement in the supercell and performing a self-consistent calculation until convergence) can be simply written under the form of an Ising Hamiltonian [32]

$$\epsilon_\alpha^{DFT} = \langle\alpha|\hat{H}|\alpha\rangle = \epsilon_0 + \frac{1}{4}\sum_{i>j} J_{ij}\sigma_i\sigma_j, \tag{4}$$

with $\sigma_i = \pm 1$. In strongly localized systems, such as $3d$ transition metal oxides, Eq. (4) can be employed to model large sets of spin configurations, and a least-squares minimization of the difference between DFT and Ising relative energies can be applied to obtain a numerical evaluation of the couplings [33,34]. In the case of β-$TeVO_4$, the determination

TABLE II. Magnetic couplings calculated using the total energy approach with four different functionals. According to the convention used in Eq. (3), positive couplings correspond to AFM interactions.

	GGA	GGA+U (AMF)	GGA+U (SIC)	PBE0
J_1	−191	−28	−87	−90
J_2	−9	1	−4	−1
J_3	17	3	9	13
J_4	70	42	30	46
J_5	3	14	2	4
J_6	−7	0	−4	−2
J_7	−7	0	−4	−2
J_8	−19	1	−7	−9

of the magnetic couplings up to the eighth nearest neighbor requires the use of two 48-atom supercells obtained by doubling the unit cell along the crystal a axis ($2 \times 1 \times 1$) or along the c axis ($1 \times 1 \times 2$), respectively. Taking crystal and spin reversal symmetries into account, this leads to a total of 50 distinct spin configurations, 22 for the $1\times1\times2$ supercell and 28 for the $2 \times 1 \times 1$ supercell. The results of the least-squares procedure applied to this set of configurations for four different functionals, namely GGA, GGA+U either within the SIC or AMF scheme, and hybrid PBE0 are shown in Fig. 4, and the numerical values of the couplings are summarized in Table II. The excellent correlation obtained between DFT energies of the various spin configurations and the corresponding Ising expressions is clearly visible in Figs. 4(a) to 4(d), independently from the actual functional employed in the calculations. A standard deviation of $\sigma \approx 4$ K is indeed obtained in the four cases, demonstrating the relevance of the mapping procedure employed here.

All the calculations tend to confirm the results obtained previously from the model Hamiltonian approach, assessing the presence of ferromagnetic nearest-neighbor and antiferromagnetic second-nearest-neighbor couplings along the chains. Large variations are observed, however, in the amplitude of the couplings with the exchange-correlation functional employed in the calculations, emphasizing the semiquantitative nature of DFT results when applied to the prediction of magnetic properties of solids. While GGA-PBE usually overestimates the amplitude of magnetic couplings as other local or semilocal functionals [35], it has been recently shown that the choice of double-counting correction schemes in DFT+U can also have a rather strong consequence on the amplitude and even the sign of short-range couplings, in particular for geometries where direct exchange can occur [23]. Our results confirm most of these aspects: GGA provides couplings about twice as large as those obtained using functionals designed to improve the treatment of strongly correlated systems. Large differences are also found between AMF and SIC versions of DFT+U, particularly on the amplitude of the nearest-neighbor interaction. It should be mentioned here that AMF calculations are in close agreement with the results obtained based on the perturbative treatment of multiorbital Hubbard model presented above. If the large dispersion of the results, particularly on the amplitude of J_1, prevents us from assessing

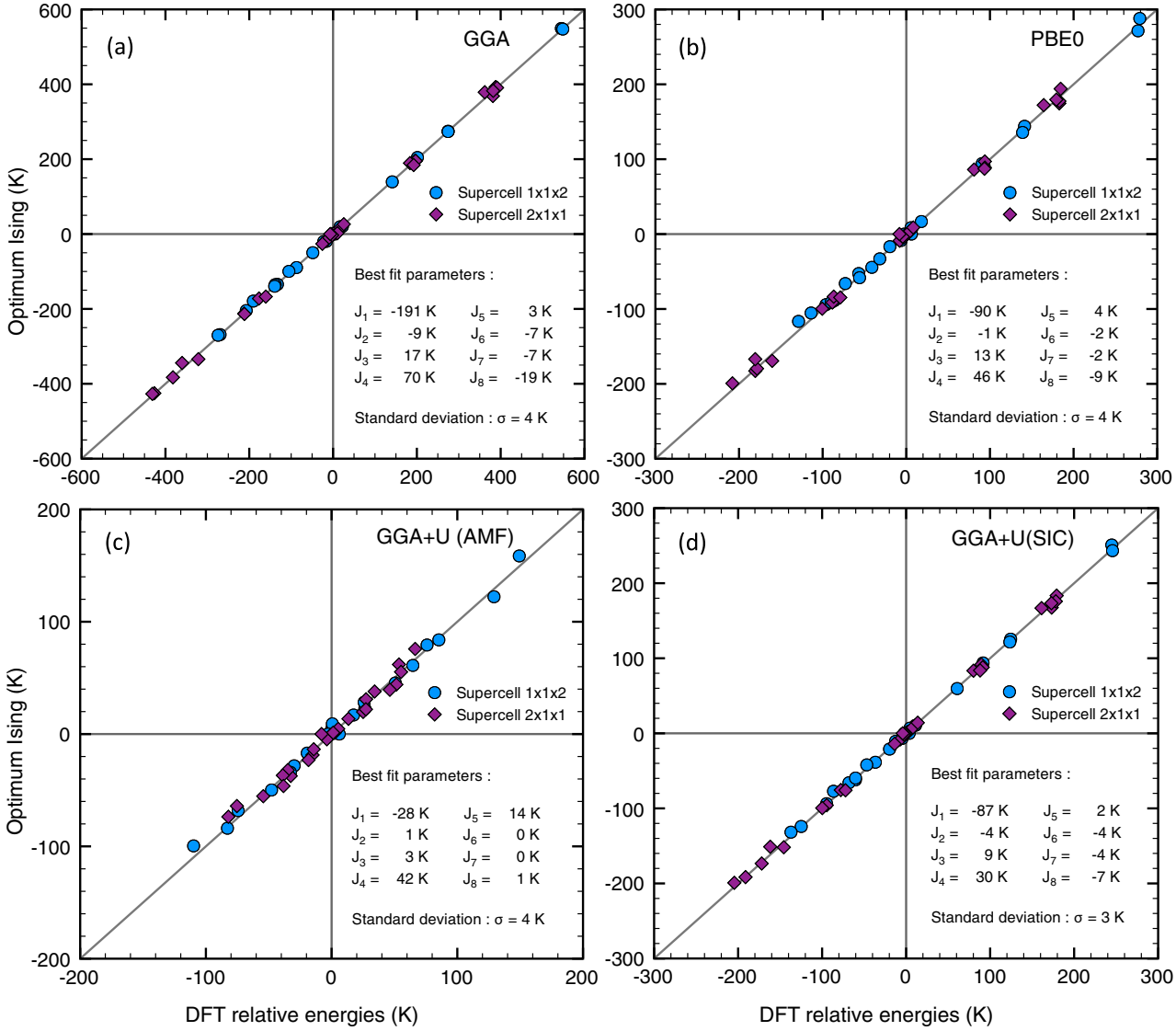

FIG. 4. (Color online) Determination of the magnetic couplings by the method of total energy differences. For each configuration, the DFT relative energy is represented versus the optimized Ising energy. The best-fit values are given in the inset. According to the convention used in Eq. (3), positive couplings correspond to AFM interactions.

a definite value of the ratio $\alpha = J_4/J_1$, all these results agree on the magnetically frustrated nature of this system.

As already mentioned, these results are rather different from the uniform AFM chain model proposed previously to interpret the temperature dependence of the magnetic susceptibility [13]. Different factors might be at the origin of this discrepancy and affect our calculations.

First, magnetic couplings are very sensitive to the detailed atomic structure of the compound under consideration. In order to investigate this point in the present case, structural relaxation has been carried out in PBE-GGA for paramagnetic β-$TeVO_4$ and the magnetic couplings have been recalculated. Although substantial variations of the amplitudes were observed, the sign of the dominant interactions along the chains remained unchanged. Second, the possibility of a change in the symmetry of the magnetically active V-3d orbital [14] was investigated by artificially increasing the distance between the vanadium and the apical oxygen atoms. Even for unrealistically large vanadyl bond length, no orbital reordering was observed. This is consistent with the large crystal-field stabilization ($\sim$1 eV) of the V-d_{xy} orbital visible in Fig. 2. Third, as mentioned above, large variations in the amplitude of the ferromagnetic nearest-neighbor coupling J_1 have been observed (a factor $\sim$3 is obtained between AMF and SIC versions of GGA+U). Assuming that this coupling cannot be correctly calculated and that its actual amplitude is much weaker than that of the second-nearest neighbor ($|J_1| \ll |J_4|$), β-$TeVO_4$ would get closer to the uniform AFM chain model proposed earlier with a single, nonnegligible intrachain coupling J_4. This model is however unable to explain the slightly positive Curie-Weiss temperature obtained for this compound, indicating the presence of balanced interactions.

We should stress here the fact that the determination of a magnetic model on the basis of a fit of the measured susceptibility is often hampered by the existence of multiple, equally satisfying solutions. The quasi-one-dimensional

helimagnet $LiCuVO_4$ is now known to be a weakly coupled frustrated ferromagnetic chain system, both experimentally from inelastic neutron scattering and theoretically from DFT calculations [36,37], but has been initially presented as a uniform AFM chain system [38,39]. Similarly, a good fit of the magnetic susceptibility of $NaCu_2O_2$ can be obtained with a uniform AFM chain model whereas the incommensurate magnetic helix ground state of this compound is explained only when accounting for a ferromagnetic nearest-neighbor and an antiferromagnetic second-nearest-neighbor couplings along the chains [40]. The spin chains in these two systems arise from edge-sharing CuO_4 plaquettes with Cu-O-Cu angles close to 90°. It is therefore reasonable to expect a weak ferromagnetic nearest-neighbor coupling in such cases. As mentioned previously, even the prediction of the signs of the magnetic interactions in β-$TeVO_4$ on the basis of such simple geometrical arguments is far from obvious and requires further experimental investigations. In particular, neutron diffraction could be envisaged to determine the nature of the long-range magnetic order below T_N.

IV. SUMMARY

In conclusion, density functional calculations have been carried out to investigate the magnetic properties of β-$TeVO_4$. In particular, two distinct approaches have been employed to evaluate magnetic couplings in this compound, based either on a perturbative treatment of the multiorbital Hubbard model in the strongly correlated limit or on the calculation of supercell total energy differences. A picture of weakly coupled frustrated ferromagnetic chains emerges from these calculations and is different from the uniform AFM chain model proposed previously for this compound [13]. We hope that these results will stimulate further experimental investigations of the puzzling magnetic properties of β-$TeVO_4$.

ACKNOWLEDGMENTS

This work was granted access to the HPC resources of IDRIS under the allocations 2013-100172 and 2014-100384 made by GENCI (Grand Equipement National de Calcul Intensif). We would like to thank Anatoli Stepanov for fruitful discussions and for bringing our attention to this compound. This work has been carried out within the framework of the ICoME2 Labex (ANR-11-LABX-0053) and the A*MIDEX projects (ANR-11-IDEX-0001-02) cofunded by the French program "Investissements d'Avenir" which is managed by the ANR, the French National Research Agency.

[1] P. Y. Zavalij and M. S. Whittingham, Acta Crystallogr., Sect. B **55**, 627 (1999).
[2] Y. Ueda, Chem. Mater. **10**, 2653 (1998).
[3] M. Isobe and Y. Ueda, J. Phys. Soc. Jpn. **65**, 1178 (1996).
[4] W. E. Pickett, Phys. Rev. Lett. **79**, 1746 (1997).
[5] R. Valentí, T. Saha-Dasgupta, J. V. Alvarez, K. Požgajčić, and C. Gros, Phys. Rev. Lett. **86**, 5381 (2001).
[6] M. A. Korotin, I. S. Elfimov, V. I. Anisimov, M. Troyer, and D. I. Khomskii, Phys. Rev. Lett. **83**, 1387 (1999).
[7] J. B. Goodenough, Phys. Rev. **100**, 564 (1955).
[8] J. B. Goodenough, J. Phys. Chem. Solids **6**, 287 (1958).
[9] J. Kanamori, J. Phys. Chem. Solids **10**, 87 (1959).
[10] P. W. Anderson, Phys. Rev. **115**, 2 (1959).
[11] Throughout this paper, we use the system of coordinates shown in Fig. 1(a) where the local z axis is oriented along the vanadyl bond, i.e., along the bond between the V and the apical O, whereas the x and y axes are approximately oriented along the bonds between V and basal O.
[12] G. Meunier, J. Darriet, and J. Galy, J. Solid State Chem. **6**, 67 (1973).
[13] Yu. Savina, O. Bludov, V. Pashchenko, S. L. Gnatchenko, P. Lemmens, and H. Berger, Phys. Rev. B **84**, 104447 (2011).
[14] V. Gnezdilov, P. Lemmens, D. Wulferding, Yu. Pashkevich, K. Lamonova, K.-Y. Choi, O. Afanasiev, S. Gnatchenko, and H. Berger, Low Temp. Phys. **38**, 559 (2012).
[15] P. Giannozzi, S. Baroni, N. Bonini, M. Calandra, R. Car, C. Cavazzoni, D. Ceresoli, G. L. Chiarotti, M. Cococcioni, I. Dabo, A. Dal Corso, S. Fabris, G. Fratesi, S. de Gironcoli, R. Gebauer, U. Gerstmann, C. Gougoussis, A. Kokalj, M. Lazzeri, L. Martin-Samos, N. Marzari, F. Mauri, R. Mazzarello, S. Paolini, A. Pasquarello, L. Paulatto, C. Sbraccia, S. Scandolo, G. Sclauzero, A. P. Seitsonen, A. Smogunov, P. Umari, and R. M. Wentzcovitch, J. Phys.: Condens. Matter **21**, 395502 (2009).
[16] P. Blaha, K. Schwarz, G. Madsen, D. Kvaniscka, and J. Luitz, in *Wien2k, An Augmented Plane Wave Plus Local Orbitals Program for Calculating Crystal Properties*, edited by K. Schwarz (Vienna University of Technology, Vienna, 2001).
[17] J. P. Perdew, K. Burke, and M. Ernzerhof, Phys. Rev. Lett. **77**, 3865 (1996).
[18] K. F. Garrity, J. W. Bennett, K. M. Rabe, and D. Vanderbilt, Comput. Mater. Sci. **81**, 446 (2014).
[19] A. A. Mostofi, J. R. Yates, Y.-S. Lee, I. Souza, D. Vanderbilt, and N. Marzari, Comput. Phys. Commun. **178**, 685 (2008).
[20] P. Novák, F. Boucher, P. Gressier, P. Blaha, and K. Schwarz, Phys. Rev. B **63**, 235114 (2001).
[21] M. T. Czyżyk and G. A. Sawatzky, Phys. Rev. B **49**, 14211 (1994).
[22] V. I. Anisimov, I. V. Solovyev, M. A. Korotin, M. T. Czyżyk, and G. A. Sawatzky, Phys. Rev. B **48**, 16929 (1993).
[23] A. A. Tsirlin, O. Janson, and H. Rosner, Phys. Rev. B **84**, 144429 (2011).
[24] R. Nath, A. A. Tsirlin, E. E. Kaul, M. Baenitz, N. Buttgen, C. Geibel, and H. Rosner, Phys. Rev. B **78**, 024418 (2008).
[25] M. Ernzerhof and G. Scuseria, J. Chem. Phys. **110**, 5029 (1999).
[26] P. Novák, J. Kuneš, L. Chaput, and W. E. Pickett, Phys. Status Solidi (b) **243**, 563 (2006).
[27] F. Tran, P. Blaha, K. Schwarz, and P. Novák, Phys. Rev. B **74**, 155108 (2006).
[28] K. I. Kugel and D. I. Khomskii, Sov. Phys. Usp. **25**, 231 (1982).
[29] V. V. Mazurenko, F. Mila, and V. I. Anisimov, Phys. Rev. B **73**, 014418 (2006).

[30] N. Marzari and D. Vanderbilt, Phys. Rev. B **56**, 12847 (1997).
[31] A. A. Tsirlin and H. Rosner, Phys. Rev. B **83**, 064415 (2011).
[32] G. Radtke, A. Saúl, H. A. Dabkowska, G. M. Luke, and G. A. Botton, Phys. Rev. Lett. **105**, 036401 (2010).
[33] A. Saúl and G. Radtke, Phys. Rev. Lett. **106**, 177203 (2011).
[34] A. Saúl, D. Vodenicarevic, and G. Radtke, Phys. Rev. B **87**, 024403 (2013).
[35] R. L. Martin and F. Illas, Phys. Rev. Lett. **79**, 1539 (1997).
[36] M. Enderle, C. Mukherjee, B. Fåk, R. K. Kremer, J.-M. Broto, H. Rosner, S.-L. Drechsler, J. Richter, J. Malek, A. Prokofiev, W. Assmus, S. Pujol, J.-L. Raggazzoni, H. Rakoto, M. Rheinstädter, and H. M. Rønnow, Europhys. Lett. **70**, 237 (2005).
[37] H.-J. Koo, C. Lee, M.-H. Whangbo, G. J. McIntyre, and R. K. Kremer, Inorg. Chem. **50**, 3582 (2011).
[38] A. N. Vasilev, JETP Lett. **69**, 876 (1999).
[39] A. N. Vasilev, L. A. Ponomarenko, H. Manaka, I. Yamada, M. Isobe, and Y. Ueda, Phys. Rev. B **64**, 024419 (2001).
[40] L. Capogna, M. Mayr, P. Horsch, M. Raichle, R. K. Kremer, M. Sofin, A. Maljuk, M. Jansen, and B. Keimer, Phys. Rev. B **71**, 140402(R) (2005).